NEW CFD BASED MODEL FOR THE DESIGN AND OPTIMISATION OF POROUS BURNERS FOR BIOMASS COMBUSTION PLANTS

G. Knauss, G. Thek, F. Biedermann, I. Obernberger
BIOS BIOENERGIESYSTEME GmbH
Hedwig-Katschinka-Straße 4, 8020, Graz Austria
Phone: +43 316 481300 68, Fax: +43 (0)316 481300 4; E-mail: knauss@bios-bioenergy.at

ABSTRACT: As no reliable CFD models for porous burners are available, a Computational Fluid Dynamics (CFD) based simulation model has been developed which is intended to serve as an innovative tool to extend the application of porous burners to biomass boilers and to support the development of this new application by CFD simulations. The model developed allows a realistic three-dimensional calculation of the combustion processes inside porous burners coupling gas phase combustion and the solid porous medium. Following the model development, a detailed validation of the new CFD model has been performed. The motivation for this work is to enable a targeted and cost-efficient computer-aided design and evaluation of porous burners as well of relevant influencing parameters in their performance.
Keywords: computational fluid dynamics (CFD), modelling, porous burner, radiation, ANSYS Fluent, non-equilibrium model, UDF, biomass, combustion.

1 INTRODUCTION AND OBJECTIVES

Combustion processes remain a challenge for companies and research institutions despite of the technical progress of the past years. The development of innovative combustion systems is getting more and more important in times of rising energy costs and decreasing emission limits.

Advanced combustion technologies such as combustion within porous burners are already used in oil and gas fired applications. The potential of porous burners for many applications in the industry is large. The technology is also already used in the steel production, the plastic and rubber production, the ceramic treatment and in the textile, paper and the food industry [1].

Their application in biomass combustion plants is new, as porous burners need a rather dust free flue gas in order to avoid plugging. New low dust biomass boiler technologies fulfil these demands and, thus, open the possibility to apply porous burners.

Porous burners can contribute to a considerable reduction in furnace volume needed, to the avoidance of local hot spots due to their good heat conductivity and to emission reduction (operating principle of a porous burner see Figure 1). Nevertheless, in order to be applied effectively, a good pre-mixing of combustible flue gas and air is needed to ensure rather homogeneous conditions at the inflow cross section of the porous burner.

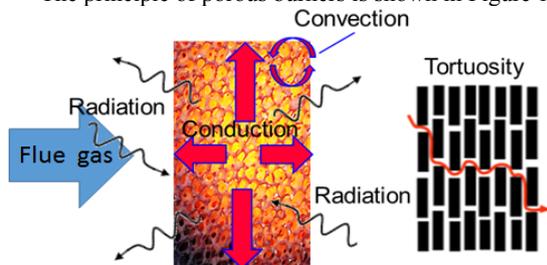The principle of porous burners is shown in Figure 1.

Figure 1: Heat transfer mechanisms inside porous burners (left); schematic explanation of a tortuous path through a porous medium.

The porous material is heated up by the radiative and convective thermal energy received from the gas phase reactions. Due to the high thermal conductivity of the porous material and the foam structure, axial as well radial heat conduction inside the porous burner can take place.

Together with the high radiative emissivity of the porous material temperature gradients in the flue gas can be reduced in areas of colder streaks. Additionally concentration gradients in the flow field are lowered by the flow through the tortuous paths which support a certain cross mixing. Together these effects lead to improved reaction conditions inside and downstream the porous burner.

With the increasing computing power of simulation computers in the past decades, new design tools for the 3D CFD simulation of combustion processes have been developed. Nowadays it is possible to perform CFD simulations of complex combustion chambers ranging from woodstoves up to biomass combustion plants with a thermal heat output up to 100 MW.

Figure 2: Porous burner (8-10 PPI) as used for the test run for the model validation

Despite the progress in computing power it is not yet possible to simulate the complex geometries of porous burners (see Figure 2) directly using common simulation computers. Therefore, models for the description of such applications are needed.

Because of that reasons a CFD model has been developed which is intended to support the new application of porous burners in biomass combustion plants. The model is intended to be able to evaluate the performance as well as relevant influence parameters for an efficient design of porous burners.

That includes the realistic calculation of the heat exchange processes inside porous burners and the interaction with its surrounding as well as the laminar flow conditions inside the porous medium.

Following the model development, a detailed model validation of the new CFD model based on test measurements in a testing plant has been performed.

2 NOMENCLATURE

2.2 Abbreviations
CFD   computational fluid dynamics
d.b.   dry base
DO   discrete ordinates
DRM   detailed reaction mechanism
EDC   eddy dissipation concept
FRK   finite rate kinetics
IR   incident radiation
KIT   Karlsruhe Institute of Technology
PB   porous burner
PIM   porous inert media
PSZ   partially stabilized zirconia
PPI   pores per inch
RTE   radiative transfer equation
SIC   silicon carbide
UDF   user defined function

2.3 Variables
a heat transfer coefficient [W/m² K]
Ab   absorptance of the PIM [-]
a_v volumetric heat transfer coefficient [W/m³ K]
C_2 inertial resistance coefficient [1/m]
C_p specific heat [J/kg K]
d diameter [m]
D_m molecular diffusion coefficient [kg/m²]
D_m' effective molecular diffusion coefficient [kg/m²]
$D_{r,eff}$ radial dispersion coefficient [kg/m²]
I irradiation intensity [W/m²]
l length [m]
Nu_v volumetric Nusselt number [-]
n refractive index [1/m]
$Pe_{m,0}$ Peclet number [-]
Q_i source term for momentum equation [N/m³]
r position vector [m]
s energy source term [W/m³]
$\vec{s}$ direction vector [m]
s' scattering direction vector [-]
S_v surface / volume ratio of the PIM [m²/m³]
T temperature [K]
U_0 superficial velocity related to the diameter of the PIM [m/s]

Greek symbols
α absorption coefficient [1/m]
β extinction coefficient [1/m]
γ permeability [m²]
δ inertial resistance coefficient (Darcy)[1/m]
ε porosity [-]
λ thermal conductivity [W/m K]
μ dynamic viscosity [kg/m s]
ν velocity [m/s]
ξ solid fraction [-]
ρ density [kg/m³]
σ Stefan–Boltzmann constant [W/m² K^4]
σ^{scat} scattering coefficient [1/m]
Ω solid angle [°]

2.3 Subscripts
char   characteristic
comp   compensation
g   gas
h   hydraulic
p   pore

PIM   porous inert media
pore   related to the pore
s   solid

2.4 Superscripts
conv   convection
rad   radiation

3 DESCRIPTION OF THE MODEL

3.1 Problem statement

The CFD codes currently available enable the simulation of the gas phase combustion and its thermal interaction with surrounding solids such as furnace or tube walls or isolation materials. The complex geometry of porous burners cannot be resolved in detail in CFD simulations (both due to their complex structure and due to limitations regarding the mesh size). Therefore, they have to be considered as porous zones in the CFD simulation. In conventional CFD routines porous zones can be implemented, where parameters such as pressure loss or overall heat conductivity can easily be considered. However, for porous burners not only pressure loss and heat conductivity are of relevance, but also the solid-solid radiation heat transfer, the gas-solid radiation heat transfer, the convective heat transfer between gas and solid, the heat conduction inside the porous material, and the influence of the tortuosity. Moreover, also the laminar flow conditions inside the pores need to be considered [3]. The pressure loss of the porous medium is considered by the Darcy-Forchheimer equation.

Since it is assumed, that especially at the entry of the flue gas into a porous burner (preheating zone) and in the reaction zone, the flue gas is not in thermal equilibrium with the porous material [2], for the modelling of porous burners, these complex heat transfer processes inside the porous burner and between the flue gas and the porous material have to be considered.

Therefore, the modelling of the radiative and convective heat exchange inside the porous burner coupled with the thermal conduction inside the porous medium were the main tasks of this work.

The porous burner model has been implemented using the commercial CFD software ANSYS Fluent. In this framework, the equations governing the temperature distribution inside the porous medium, the interaction between the solid and fluid phase and the flow regime have been implemented by use of the corresponding scalar transport equations and User Defined Functions (UDFs).

3.2 Gas phase models

In a combustion process heat and mass transfer play an important role, whereas in most cases the modelling of the gas phase is completely solved by the standard CFD code. For describing the flue gas flow inside the porous burner the newly developed model relies mainly on the build-in features of ANSYS Fluent.

The present model is based on the EDC model to describe the turbulence-chemistry interaction. The gas phase reactions are calculated based on the DRM 22 mechanism, which is a reduced GRI-Mech mechanism [5].

An in-house developed hybrid gas phase reaction model suitable for laminar to highly turbulent flows has been applied for the simulation of the reacting gas flow in the entire combustion chamber. The model calculates the effective reaction rates from laminar finite rate kinetics (FRK) and the turbulent reaction rates and weights them

depending on the local turbulent Reynolds number of the flow field [6].

Laminar flow conditions inside the pores are assumed in case of low superficial velocities and high PPI numbers (>10 PPI) [7]. The authors show a significant laminarisation effect due to porous media which rises with decreasing pore diameter. Experiments performed by [3] based on synthetically produced porous media revealed that no laminar-turbulent transition has to be expected in the area between 10 and 100 PPI for Reynolds numbers (Re_p) up to 1,100. For the CFD model, therefore, a laminar flow in the porous body was assumed. To consider the laminar flow reactions inside the porous burner the Finite Rate Kinetics model was permanently activated inside the porous zone.

The porous zone model of ANSYS Fluent introduces a momentum source which requires coefficients for permeability and internal resistance [8]. Equation. (**1**) represents the source term for the momentum equation of a homogeneous porous medium as it is used in ANSYS Fluent. This momentum sink contributes to the pressure gradient in the porous cell where $1/\gamma$ is the permeability and C_2 is the internal resistance. In the model developed these input parameters for the porous zone model are calculated based on the Darcy-Forchheimer equation (**2**), where again $1/\gamma$ is the permeability of the porous medium, δ is the inertial resistance coefficient, μ is the dynamic viscosity, ρ is the density, l is the thickness of the porous body and ν the superficial velocity. Values for δ and γ were provided by the Karlsruhe Institute of Technology (KIT), the producer of the porous medium which was used for the test runs and the model validation.

$$Q_i = -\left(\frac{\mu}{\gamma} v_i + C_2 \cdot \frac{1}{2} \cdot \rho \cdot |v| \cdot v_i \right) \tag{1}$$

$$\Delta p = \frac{\mu}{\gamma} \cdot l \cdot v + \delta \cdot \rho \cdot l \cdot v^2 \tag{2}$$

3.3 Radiation model of the solid phase

The ANSYS Fluent internal energy transport equation comprises terms and parameters describing the heat transfer (Eq. (**3**)). Here λ_{PIM} is the effective thermal conductivity of the porous medium (including voids), ε is the solid fraction, ρ_P is the density of the PIM, T_s is the solid temperature, C_P is the specific heat and S_s is the energy source introduced for the convective and the radiative heat transfer (Eq. (**4**)).

$$\frac{\partial(\xi \rho_P C_P T_S)}{\partial T} = \nabla(\lambda_{PIM} \cdot \nabla T_S) + S_s \tag{3}$$

$$S_s = S_s^{conv} + S_s^{rad} \tag{4}$$

Because of the high temperatures, radiation has an important influence on the heat exchange between the solid and the gas phase inside porous burners.

In the present work the discrete ordinates radiation model (DO) is used for the modifications because of its high directional accuracy ([8] and [9]). The basic changes for the implementation of the interaction of the DO model with the solid phase are based on the work of [9] and [10].

The DO radiation model solves the radiative transfer equation (RTE) (Eq. (**5**)) for a finite number of discrete solid angles, each associated with a vector $\vec{s}$ direction fixed in the global Cartesian system [8]. Here α_s and α_g are the absorption coefficients of the solid (PIM) and the gas phase, n is the refractive index, σ is the Stefan–Boltzmann constant, σ^{scat} is the scattering coefficient and T_g and T_s are the gas and the solid (PIM) temperature.

$$\nabla I(r,s) + (\alpha + \sigma^{scat}) I(r,s) = \frac{\alpha \cdot n^2 \cdot \sigma \cdot T_g^4}{\pi} + $$
$$\frac{\sigma^{scat}}{4\pi} \int_0^{4\pi} I(r,s') \Phi(s,s') d\Omega \tag{5}$$

In a single phase medium ANSYS Fluent solves the radiative transport equation and introduces an energy source in the gas phase. This represents the radiative emittance and absorbance of each cell (Eq. (6). To consider a two-phase medium some changes had to be introduced into the model. For the implementation of the radiative heat transfer between gas and solid phase an energy source term for the solid phase was implemented via UDF (Eq. (7)).

$$S_g^{rad} = \int_0^{4\pi} \left(\alpha_g \cdot I(r,s) - \frac{\alpha_g \cdot n^2 \cdot \sigma \cdot T_g^4}{\pi} \right) d\Omega \tag{6}$$

$$S_s^{rad} = \int_0^{4\pi} \left(\alpha_s \cdot I(r,s) - \frac{\alpha_s \cdot n^2 \cdot \sigma \cdot T_s^4}{\pi} \right) d\Omega \tag{7}$$

Now the radiative transfer equation had to be modified to receive the same equation as (Eq. (**5**)) but also considering the solid phase of the PIM (Eq. (**10**)). Therefore the absorption and the scattering coefficient had to be extended by the absorption and scattering coefficient of the solid phase (Eq. (**8**) and (**9**) [9].

$$\alpha = \alpha_s + \alpha_g, \tag{8}$$

$$\sigma^{scat} = \sigma_s^{scat} + \sigma_g^{scat} \tag{9}$$

$$\nabla I(r,s) + (\alpha_s + \alpha_g + \sigma_s^{scat} + \sigma_g^{scat}) I(r,s)$$
$$= \frac{\alpha_s \cdot n^2 \cdot \sigma \cdot T_s^4}{\pi} + \frac{\alpha_g \cdot n^2 \cdot \sigma \cdot T_g^4}{\pi} + \frac{\sigma_s^{scat} + \sigma_g^{scat}}{4\pi} \int_0^{4\pi} I(r,s') \Phi(s,s') d\Omega \tag{10}$$

By the replacement of the absorption coefficient (Eq. (8)) via UDF, ANSYS Fluent internally also changes the energy source of the gas from Eq. (6) to Eq. (11).

$$S_g^{rad} = \int_0^{4\pi} \left((\alpha_s + \alpha_g) \cdot I(r,s) - \frac{(\alpha_s + \alpha_g) \cdot n^2 \cdot \sigma \cdot T_g^4}{\pi} \right) d\Omega \tag{11}$$

For the correction of equation (11) and to receive equation (6), the part scaled with the solid absorption coefficient has to be subtracted from the gas phase using a compensation source which has the form of (14).

$$\overset{\bullet}{S}_g^{rad} = \int_0^{4\pi} \left((\alpha_s + \alpha_g) \cdot I(r,s) - \frac{(\alpha_s + \alpha_g) \cdot n^2 \cdot \sigma \cdot T_g^4}{\pi} \right) d\Omega \tag{12}$$

$$S_g^{rad} = S_g^{rad} + S_{comp} \tag{13}$$

$$S_{comp} = \int_0^{4\pi} \left(-\alpha_s \cdot I(r,s) - \frac{\alpha_s \cdot n^2 \cdot \sigma \cdot T_g^4}{\pi} \right) d\Omega \tag{14}$$

Also when the physical velocity formulation of the porous zone is activated, the radiation source of the gas phase is scaled with the porosity defined for the porous zone. This leads to an imbalance between RTE and energy equation (also in the standard DO model of ANSYS Fluent) [8], [9], [10]. Thus for a closed energy balance the compensation source (Eq. (**13**)) had to be extended by a correction term for the porosity (Eq.

(**15**)). After the consideration of the correction equation the radiation source in the original form follows for the gas phase (Eq.(**6**) [10].

$$S_g^{rad} = (1-\varepsilon) \overset{\bullet}{S}_g^{rad} + S_{comp} \tag{15}$$

Different models for the calculation of the extinction coefficient of porous bodies are available in literature. The authors of [11] derive an empirical formulation for the extinction coefficient of a solid sponge as a function of structural characteristics. In [12] the equation is modified based on own measurement data for both, PSZ and SiC sponges (Eq.(16)). This approach is also used for modelling in the present work.

$$\beta_s = \frac{4.4}{d_{pore}} \cdot (1 - \varepsilon) \quad (16)$$

[13] provides the relationship between the extinction coefficient (β_s), the absorption coefficient α_s, the scattering coefficient σ_s^{scat}, and the absorptance (Ab) of the solid fraction (Eq. (17) and (18)). In the present CFD model, the scattering coefficient of the gas phase is neglected.

$$\beta_S = \alpha_s + \sigma_s^{scat} \quad (17)$$

$$\alpha_S = Ab \cdot \beta_s \quad (18)$$

3.4 Modelling the thermal conductivity of the PIM

Studies on the determination of the effective thermal conductivity (excluding radiation influences) were carried out by [14] based on structural models. The authors derived a model which represents a formulation of the effective thermal conductivity as a function of the thermal conductivity of the dense material and the porosity of the porous medium (Eq. (19) and (20)). For the modelling of the thermal conductivity inside the porous zone this formulation was integrated into the ANSYS Fluent internal transport equation (3) of the temperature, and is considered in the cell zone of the porous medium.

$$\lambda_{PIM} = \frac{1}{\sqrt{2}} \cdot \left(\frac{4 \cdot k}{2 \cdot e^2 + \pi \cdot k \cdot (1-e)} + \frac{3e-2k}{e^2} + \frac{(\sqrt{2}-2e)^2}{2 \cdot \pi \cdot k^2 \cdot (1-2e \cdot \sqrt{2})} \right)^{-1} \quad (19)$$

$$k = \sqrt{\frac{\sqrt{2} \cdot (2 - \frac{5}{8} \cdot e^3 \cdot \sqrt{2} - 3 \cdot \varepsilon)}{\pi \cdot (3 - 4 \cdot e \cdot \sqrt{2} - e)}}, \quad e = 0.339 \quad (20)$$

3.5 Model for the convective heat transfer between gas and solid.

Since it is difficult to determine the geometric surface inside porous media, the volumetric heat transfer coefficient a_v based on the specific surface area (S_v) is usually used as suggested by [15] (Eq. (21))

$$a_V = a \cdot S_V \quad (21)$$

The volumetric Nusselt number Nu_V including the volumetric heat transfer coefficient a_v is defined as Eq. (22). As suggested by [15], d_{char} represents the real pore diameter. In order to compensate the volume unit in a_v, the characteristic length of the Nusselt correlation appears untypically with the second power.

$$Nu_V = \frac{a_v \cdot d_{char}^2}{\lambda_g} \quad (22)$$

In [15] a correlation for the determination of the volumetric Nusselt number (without influences of radiation) (Eq. (23)) has been derived, where L is the length of the porous body in flow direction and Re is the volumetric Reynolds number, which is defined as (Eq. (24)). Together with Eq. (22) the volumetric heat transfer coefficient is given and can be substituted in Eq. (25), which completes Eq. (4).

$$Nu_V = 0.819 \cdot \left[1 - 7.33 \cdot \left(\frac{d_{pore}}{L} \right) \right] \cdot Re^{0.36 \cdot \left[1+15.5 \cdot \left(\frac{d_{pore}}{L} \right) \right]} \quad (23)$$

$$Re = \frac{\rho_g \cdot U_0 \cdot d_h}{\varepsilon \cdot \mu_g} \quad (24)$$

$$S_s^{conv} = -S_g^{conv} = \alpha_v \cdot (T_g - T_s) \quad (25)$$

For a closed energy balance the convective heat transfer had to be considered for the fluid and the solid phase.

3.6 Modelling the hydrodynamic dispersion

The hydrodynamic dispersion describes the increased mixing driven by the complex three-dimensional flow field, which is present in porous media. The dispersion is caused by dividing and combining the streamlines along different tortuous paths [2]. Molecular diffusion plays a minor role in this case. For porous systems, the reduced open cross-section caused by the porosity can be taken into account with an effective molar diffusion coefficient [16] (26).

In literature the dispersion during the flow through porous media is divided into axial and radial dispersion. Experiments show that, in the case of foam ceramics, a better agreement between the experiment and the calculation model can be achieved by replacing the axial with the radial dispersion coefficient [17] (27) (especially with a short thickness of the porous medium in flow direction and independent of the pore size).

$$D_m' = D_m \cdot \left(1 - \sqrt{1-\varepsilon} \right) \quad (26)$$

In literature an approach for the axial flow dispersion in porous beds can be found (27), which was adapted for ceramic foams [16], [17]. Here the Peclet number (Equation (28)) describes the relation between convective flow and diffusion.

$$D_{r,eff} = D_m' + \frac{63}{320} \cdot \sqrt{2 \cdot (1-\varepsilon)} \cdot Pe_{m,0}' \cdot D_m' \quad (27)$$

$$Pe_{m,0} = \frac{v_p \cdot d_p}{D_m} \quad (28)$$

For the developed model of the porous burner model it was assumed that the dispersion can be described for all coordinate directions with Equation. (27).

4 TEST CASE USED FOR VALIDATION

For the validation of the newly developed model a 400 kW gas burner connected to an updraft gasifier was selected (relevant section with the porous burner shown in Figure 3), where test runs at nominal load have been performed.

As fuel, softwood chips with a moisture content of 36.5 wt.% w.b. were used. At a total air ratio of 1.28 and a flue gas recirculation ratio of 0.12, an amount of 950 kg/h flue gas with an average temperature of about 1,130°C results at the entry into the porous burner.

The gas released from the updraft gasifier is first mixed with secondary air and recirculated flue gas for conversion under reducing conditions (partial conversion in the secondary combustion zone). Before the porous burner, tertiary air is supplied in order to achieve a complete gas conversion in the tertiary combustion zone where the porous burner is located. The tertiary air nozzles are arranged tangentially to induce a rotational flow.
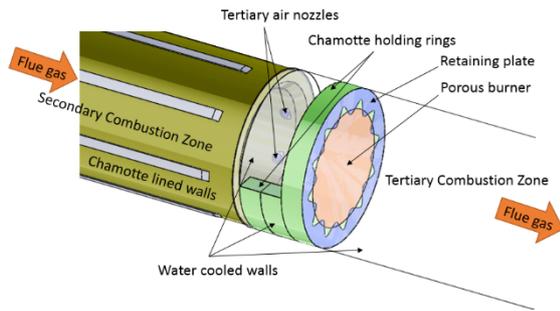
Figure 3: 3D geometry of the section where the porous burner is implemented in the burnout zone

During the test runs the plant was equipped with a porous burner (pore size 8-10 PPI) made of silicon carbide, which has been installed at the beginning of the tertiary combustion zone. The ceramic foam was provided by the Karlsruhe Institute of Technology (KIT). The most relevant material properties of the porous burner are summarized in Table 1.

Table 1: Material properties of the porous burner

Parameter	Unit	Value
Material		SiC
Thermal conductivity	[W/mK]	50 (at 1,000 °C)
Specific surface area	[m²/m³]	700
Real pore diameter	[μm]	4,500
Diameter	[mm]	348
Height	[mm]	68
Porosity	[%]	84
Density	[g/cm³]	0.4
Emissivity	[-]	0.9
Pores per inch	[PPI]	8-10

5 RESULTS AND DISCUSSION

5.1 Measurements during the test runs

During the test runs at the 400 kW gasifier the following measurements were performed:

- Pyrometer measurement of the flue gas temperatures as well as CO and O_2 concentrations at several positions in the secondary (SCZ) and the tertiary combustion zone (TCZ)
- Temperatures at two positions inside the porous burner and on its surface
- CO and O_2 concentrations at boiler outlet
- Pressure loss over the porous burner

For the validation of the simulation model the most relevant measuring positions (see MP-1 to MP-3 in Figure 4) are compared to the simulation results.
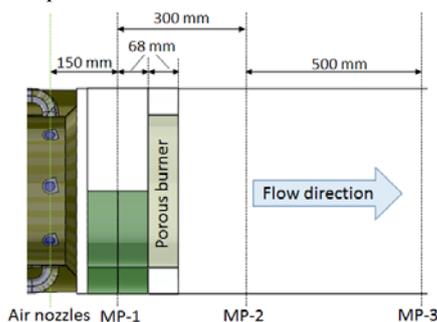

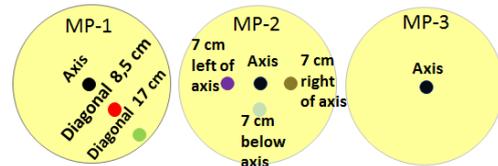Figure 4: Description of the measuring planes upstream and downstream of the porous burner

Figure 5: Description of the positions of the particular measuring points MP-1 to MP-3

5.2 Evaluation of the porous burner temperature

The tertiary air enters the combustion chamber about 220 mm upstream the porous burner. At the inlet into the porous burner the flue gas shows large gradients in temperature, CO and O_2 concentrations.

For the optical evaluation of the temperature gradients on the surface of the porous burner, pictures were taken from the direction of the TCZ and the SCZ and compared with equivalent temperature plots from the CFD simulation (see Figure 6). Both, in the results of the CFD simulations and the optical evaluation of the test runs an uneven temperature distribution can be seen on the surface of the porous burner whereby the shapes and the positions of the cooler and the hotter spots on the burner surface are in good agreement with the simulation results.
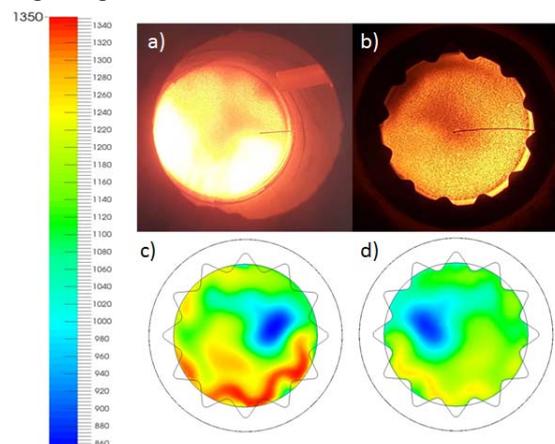

Figure 6: a): porous burner seen from the SCZ; b): porous burner seen from the TCZ; surface temperatures of the porous burner according to CFD: c): burner inlet; d): burner outlet.

Temperature measurements have been carried out in the centre of the outlet surface (see T-PIM1 in **Figure 7**) and the core of the porous burner, about five centimetres from the edge (see T-PIM2 in **Figure 7**).
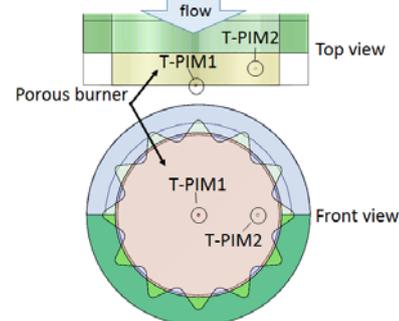

Figure 7: Temperature measurement positions in the porous burner: T-PIM1: centre of the outlet surface of the PIM; T-PIM2: in the core of the burner about 5 cm from the edge.

The measured temperature in T-PIM1 of 996 °C is in good agreement with the simulated temperature of 1,020 °C at this position. For T-PIM2 larger deviations between measurement and simulation appear (measurement: 1,251 °C; simulation: 1,150 °C) which is most likely due to the large temperature gradients because of the secondary air injected directly upstream the burner.

The comparison of the simulated average flue gas temperature and the simulated average temperature of the porous material (see Figure 8) shows that the porous burner is not in thermal equilibrium with the flue gas flow. This is in accordance with the corresponding literature [2].
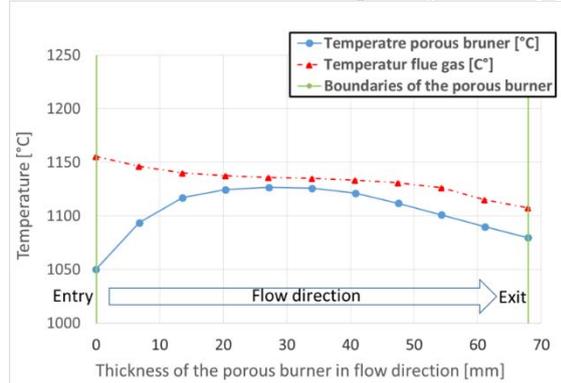

Figure 8: Average simulated PIM and flue gas temperatures inside the porous burner evaluated on eleven section planes in flow direction through the porous zone

As shown in Figure 8, according to the simulation, the flue gas enters the porous burner with an average temperature of about 1,150 °C. At this point the simulated temperature of the porous burner is about 100 °C below the gas temperature. The main reason for the lower temperatures at the inlet and outlet surface of the porous burner can be found in the radiative heat transfer from the porous burner to the SCZ and the TCZ as well as the conductive heat losses through the chamotte holding rings to the cooled boiler walls. In the simulation model, the chemical energy released by the gas phase reactions inside the porous burner is transferred to the porous material by radiation and convection.

At the measured high operating temperatures of the porous burner (>1,000 °C) the most important heat transfer mechanism is the radiative gas-solid and solid-solid heat transfer. Figure 9 represents a visualisation of the incident radiation (IR is the integral over all solid angles of the radiation intensity; [8]) inside the porous burner as well as the surrounding SCZ and TCZ for two different simulation cases. The picture on top shows the increased radiation intensity in the area around and inside the porous burner. Below, CFD results without porous model are illustrated for comparison.
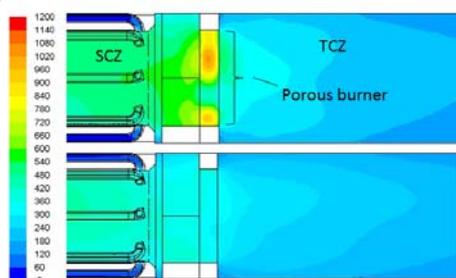

Figure 9: Incident radiation [W/m²] in a centre cut through the burner with activated (top) and de-activated (bottom) porous burner model

Due to the increased heat emission of the porous burner into the SCZ, a temperature increase in the gas before the PB can be seen in the simulation results. This effect could also be observed in comparative test runs with and without porous burner.

5.3 Evaluation of flue gas temperatures

Measurements of the flue gas temperatures at different positions in the SCZ and the TCZ have been performed. Figure 10 shows the measured temperatures in the three measuring planes MP-1 to MP-3 (see Figure 4 and Figure 5) inside the gas burner compared to the simulated average values for the temperatures including standard deviation as well minimum and maximum values in the planes evaluated.
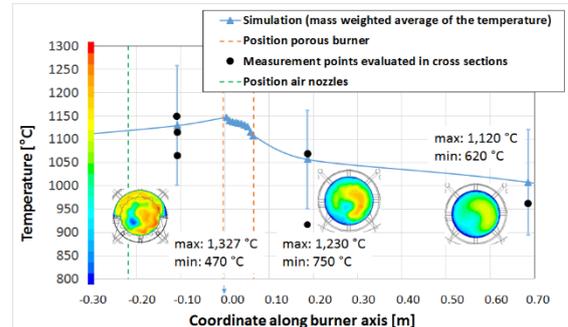

Figure 10: Temperature measurements compared to simulated average temperature values in the measurement planes.

Both, according to the simulation results and the measurement data high temperature gradients occur at the measuring position upstream the porous burner. These gradients result from the combustion air which is injected about 150 mm upstream the measurement position. Especially upstream the porous burner a pulsing flow could be observed which leaded to fluctuations in the temperature.

Due to these large gradients and an exact comparison of the measuring positions (see MP-1 to MP-3 Figure 4 and Figure 5) with the CFD results at these positions was not possible.

At measurement position MP-2 and MP-3 the flue gas temperatures are lower due to the cooled boiler walls. The measurement data as well as the simulation results indicate that also after the porous burner large temperature gradients exist. It can be assumed that the gradients cannot be homogenised by the heat transport mechanisms inside the porous burner due to the high gas throughput and resulting low residence times.

In general, the temperature measurements are in good agreement with the simulation results.

5.4 Evaluation of the O_2 concentrations in the flue gas

Measurements of the oxygen concentrations on several positions upstream and downstream the porous burner have been performed (measuring positions equal to temperature measurement). Figure 11 shows a comparison of the measured values with the average values of the simulation results in the cross sections MP-1 to MP-3 including standard deviations, minimum and maximum values.
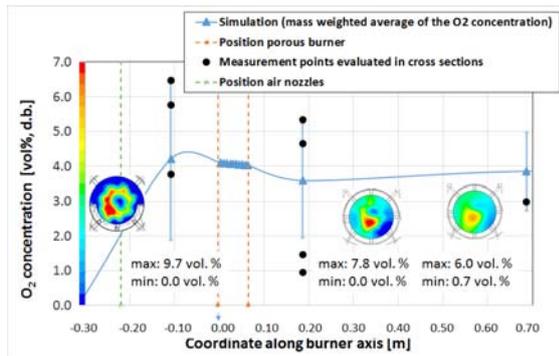
Figure 11: Measured O_2 concentrations compared to simulated average O_2 concentrations in the measurement planes

Figure 12: CO measurements compared to simulated average CO concentrations including the standard deviations in the measurement planes evaluated

Upstream the porous burner, large gradients in the oxygen concentrations of the flue gas can be seen both according to simulation results and to measurement data. These gradients are to be expected since the tertiary air is injected closely before.

At measuring positions MP-2 and MP-3 the measurement data as well as the simulation results also indicate high gradients in the O_2 concentration (measurement: ~1 to 5.5 vol.% d.b.; simulation: 2 to 5.3 vol.% d.b.). In the simulation results as well the measurement data just a low cross mixing due to the tortuosity of the porous material can be seen. This indicates a good description of the flow dispersion model used (see section 2.2).

5.5 Evaluation of the CO concentrations in the flue gas

CO measurements have been carried out at several positions at MP-1, MP-2 and MP-3 (see Figure 4). For measuring position MP-1 high CO concentration gradients with peak values of up to 49,000 ppmv d.b. can be seen based on the measurement data (see Figure 12). From the simulation results also large CO concentration gradients for this measuring position can be derived. The maximum simulated CO concentration in MP-1 amounts to 45,200 ppmv, which is in good agreement with the peak value according to measurements.

At measurement position MP-2 after the porous burner the maximum measured CO concentration reaches about 5,000 ppmv d.b. and the simulated peak value reaches about 17,400 ppmv d.b.

The simulation results as well as the measurement data indicate that the gas phase burn out at this position is still not completed. At measuring position MP-3 both the simulation as well as measurement data show a comparable burn out quality (measurement 423 ppmv d.b.; simulation 102 ppmv d.b., maximum value 240 ppmv d.b.).
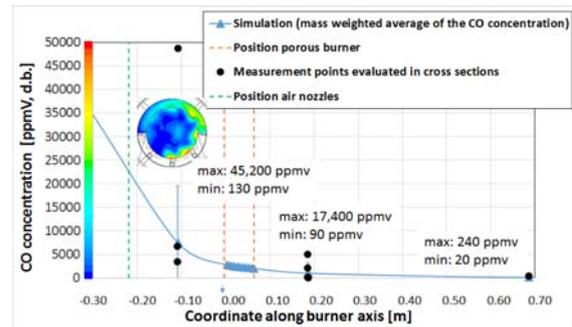
6 CONCLUSIONS AND OUTLOOK

In this work, a 3D CFD model for the simulation of porous burners, which considers the most important heat exchange mechanisms, has been developed. The temperature measurements inside the porous burner show a good agreement with the simulation results which indicates a proper modelling of the relevant heat transfer mechanisms inside the complex foam structure.

The simulation results for the CO and O_2 concentrations directly after the porous burner are also in acceptable agreement with the measured values.

Due to the pronounced swirled flow and the strong gradients at the position of the porous burner the direct comparison of measured and simulated values at single positions is difficult. Therefore, future validation work should be made on smaller facilities with a more even flow field and lower concentration gradients. Based on such laboratory scale validations, more accurate model calibrations (for example regarding the flow dispersion) could be performed.

The novel CFD model presented here opens up the opportunity for a cost-efficient computer-aided design and evaluation of porous burners as well their application in biomass combustion plants.

The model results show that for an efficient application of porous burners in biomass combustion plants the effective premixing of air and flue gas (avoid strain formation) as well as high temperatures in the porous burner are crucial to achieve good burn out conditions.

7 REFERENCES

[1] E. Reuße 2012: Innovative industrielle Erdgasbeheizungssysteme auf der Basis der Porenbrennertechnologie für Hochtemperaturanwendungen, PhD thesis at the Technischen Universität Bergakademie Freiberg.

[2] Djordjevic N, 2011: Flammenstabilisierung durch Verbrennung in festen Schwämmen, PhD thesis at the Karlsruher Institut für Technologie (KIT).

[3] D. Seguin, A Montillet, J. Comiti, 1998: Experimental characterisation of flow regimes in various porous media: Limit of laminar flow regime. In: Chemical Engineering Science 53(21):3751-3761.

[4] C. Bedoya, I. Dinkov, P. Habisreuther, N. Zarzalis, H. Bockhorn, P. Parthasarathy, 2015: Experimental study, 1D volume-averaged calculations and 3D direct pore level simulations of the flame

stabilization in porous inert media at elevated pressure. In: Combustion and Flame 15(000):41-1.

[5] http://combustion.berkeley.edu/drm/drm22.dat

[6] A. Shiehnejadhesar, R. Mehrabian, R. Scharler, I. Obernberger, 2015: Development of a streak formation model for an improved prediction of gas phase combustion in biomass grate furnaces. 10th European Conference on Industrial Furnaces and Boilers, At Porto, Portugal.

[7] Hall, M. J., Hiatt, J.P: Measurements of pore scale flows within and exiting ceramic foams. Experiments in Fluids 20, 433-440 (1996).

[8] ANSYS Fluent Theory Guide Version 16.2

[9] M.A. Gómez, J. Porteiro, D. Patiño, J.L. Míguez, 2012: CFD simulation of a solar radiation absorber. In: International Journal of Heat and Mass Transfer 57(1):231–240.

[10] M.A. Gómez, D. Patiño, Roberto Comesaña, J.L. Míguez, 2014: CFD modelling of thermal conversion and packed bed compaction in biomass combustion. In: Fuel 117:716-732.

[11] Hsu, P.F., Howell, J.R 1993: Measurements of thermal conductivity and optical properties of porous partially stabilized zirconia. Experimental Heat Transfer 5, 293-313.

[12] Hendricks, T.J., Howell, J.R. 1996: Absorption/scattering coefficients and scattering phase functions in reticulated porous ceramics. J. Heat Transf. 118, 1, 79-87.

[13] M. Tancrez, J. Taine 2004: Direct identification of absorption and scattering coefficients and phase function of a porous medium by a Monte Carlo technique. In: International Journal of Heat and Mass Transfer 47(2):373-383.

[14] Boomsma, K., Poulikakos, D. 2001: On the effective thermal conductivity of a three-dimensionally structured fluid-saturated metal foam. Int. J. Heat Mass Transfer, 44, 827-836.

[15] Younis, L.B., Viskanta, R. 1993: Experimental determination of the volumetric heat transfer coefficient between stream of air and ceramic foam. International Journal of Heat and Mass Transfer 36, 1425-1434.

[16] M. Endisch 2013: Experimentelle und numerische Untersuchungen zur stabilen Entsorgung von Schwachgasen in porösen Verbrennungsreaktoren, PhD thesis at the Technische Universität Bergakademie Freiberg.

[17] J.C.F. Pereira, I, 1996: Malico, T.C. Hayashi, J. Raposo. Experimental and numerical characterization of the transverse dispersion at the exit of a short ceramic foam inside a pipe. In: Experiments in Fluids 21(4):286-290.

8 LOGOSPACE